Inorg. Chem. **2008**, *47*, 9489−9496

$Sn_xPt_4Sn_ySb_{12-y}$: A Skutterudite with Covalently Bonded Filler

Y. Liang,[†,‡,§] H. Borrmann,[†] M. Baenitz,[†] W. Schnelle,[†] S. Budnyk,[†] J. T. Zhao,[‡] and Yu. Grin*[,†]

Max-Planck-Institut für Chemische Physik fester Stoffe, Nöthnitzer Str. 40, 01187 Dresden, Germany, State Key Laboratory of High Performance Ceramics and Superfine Microstructures, Shanghai Institute of Ceramics, Chinese Academic of Sciences, Dingxi Road 1295, Shanghai 200050, P. R. China, and Graduate School of the Chinese Academy of Science, Beijing, P. R. China

Received June 23, 2008

A new phase, $Sn_xPt_4Sb_{12-y}Sn_y$, has been prepared from the elements. It exhibits a wide range of homogeneity with $0.3(2) \leq x \leq 1.0(2)$ and $4.2(2) \leq y \leq 7.0(2)$. The crystal structure and the composition were established by single-crystal and powder X-ray diffraction as well as wavelength-dispersive X-ray analysis measurements and were supported by nuclear magnetic resonance experiments. The compound is the first representative of the filled-skutterudite family with the filler atoms not located at the center of the cavity but covalently bonded to the cavity's wall, as confirmed by the analysis of chemical bonding with the electron localizability indicator. The Sn and Sb atoms share the framework site with different coordinate parameters caused by the difference in atomic size; additional tin atoms are located in the cavities of the framework. The material is a diamagnet in the whole composition range. In agreement with the calculated electronic density of states, the material reveals a metallic behavior in electronic transport. The absolute values of electrical resistivity vary with the tin-to-antimony ratio.

Introduction

The mineral skutterudite was identified by Oftedal[1] in 1928 as having a body-centered cubic crystal structure belonging to the space group $Im\bar{3}$. The crystal structure contains different cavities in the basic framework. Their existence opens the opportunity to introduce additional atoms into the lattice. While the group 9 transition metals form binary skutterudite derivatives with pnicogens, binary representatives with group 8 transition metals do not exist because of the obvious bonding problems. The filler cation R is expected to supply additional electrons and saturate the bonding demands of the structural motif. The first filled skutterudite—$LaFe_4P_{12}$—was synthesized by Jeitschko and Braun.[2] Shortly thereafter, numerous filled skutterudites were prepared also in the arsenic and antimony families. Nowadays, series of compounds $R[T_4X_{12}]$ have been synthesized, where T is a metal such as Co, Fe, Ru, or Os and X represents a pnicogen like P, As, or Sb.[3−13] It is interesting to note that the icosahedral void at position 2*a* (0 0 0) can be filled not only by an alkali metal, an alkaline-earth metal, or a rare-earth metal atom but also by tin: $Sn_{1-x}Fe_4Sb_{12}$,[14] $Sn_{1-x}Co_4Sb_{12}$,[15] and $Sn_xNi_4Sn_ySb_{12-y}$.[16] In the best analyzed crystal structure of $Sn_xNi_4Sn_ySb_{12-y}$, the Sn and Sb atoms

* Author to whom correspondence should be addressed. E-mail: grin@cpfs.mpg.de.
† Max-Planck-Institut für Chemische Physik fester Stoffe.
‡ Chinese Academic of Sciences.
§ Graduate School of the Chinese Academy of Science.

(1) (a) Breithaupt, A. *Ann. Phys. (Leipzig)* **1827**, *9*, 115–116. (b) Oftedal, I. *Z. Kristallogr.* **1928**, *A66*, 517–546.
(2) Jeitschko, W.; Braun, D. *Acta Crystallogr.* **1977**, *B33*, 3401–3406.
(3) Braun, D. J.; Jeitschko, W. *J. Solid State Chem.* **1980**, *32*, 357–363.
(4) Braun, D. J.; Jeitschko, W. *J. Less-Common Met.* **1980**, *72*, 147–156.
(5) Zemni, S.; Tranqui, D.; Chaudouet, P.; Madar, R.; Senateur, J. P. *J. Solid State Chem.* **1986**, *65*, 1–5.
(6) Evers, C. B. H.; Jeitschko, W.; Boonk, L.; Braun, D. J.; Ebel, T.; Scholz, U. D. *J. Alloys Compd.* **1995**, *224*, 184–189.
(7) Jeitschko, W.; Foecker, A. E.; Paschke, D.; Dewalsky, M. V.; Evers, Ch. B. H.; Kunnen, B.; Lang, A.; Kotzyba, G.; Rodewald, U. Ch.; Moller, M. H. *Z. Anorg. Allg. Chem.* **2000**, *626*, 1112–1120.
(8) Watcharapasorn, A.; Feigelson, R. S.; Caillat, T.; Borshchevsky, A.; Snyder, G. J.; Fleurial, J.-P. *J. Appl. Phys.* **2002**, *91*, 1344–1348.
(9) Shirotani, I.; Shimaya, Y.; Kihou, K.; Sekine, C.; Yagi, T. *J. Solid State Chem.* **2003**, *174*, 32–34.
(10) Kihou, K.; Shirotani, I.; Shimaya, Y.; Sekine, C.; Yagi, T. *Mater. Res. Bull.* **2004**, *39*, 317–325.
(11) Shirotani, I.; Hayashi, J.; Takeda, K.; Nakada, R.; Ohishi, Y. *Physica B (Amsterdam, Neth.)* **2006**, *382*, 8–12.
(12) Lee, C. H.; Matsuhata, H.; Yamaguchi, H.; Sekine, C.; Suzuki, T.; Noro, T.; Shirotani, I. *Phys Rev. B: Condens. Matter Mater. Phys.* **2004**, *70*, 153105(1−4).
(13) Leithe-Jasper, A.; Schnelle, W.; Rosner, H.; Senthilkumaran, N.; Rabis, A.; Baenitz, M.; Gippius, A.; Morozova, E.; Mydosh, J. A.; Grin, Yu. *Phys. Rev. Lett.* **2003**, *91*, 037208(1−4).

10.1021/ic801154a CCC: $40.75
Published on Web 09/24/2008

Table 1. Composition and Lattice Parameters of $Sn_xPt_4Sn_ySb_{12-y}$

composition		
starting	according to WDXS/EDXS	lattice parameter (Å)
$Sn_{0.4}Pt_4Sn_{7.0}Sb_{5.0}$		9.3924(2)
$Sn_{0.4}Pt_4Sn_{6.0}Sb_{6.0}$		9.3708(3)
$Sn_{0.4}Pt_4Sn_{4.8}Sb_{7.2}$		9.3503(2)
$Sn_{1.0}Pt_4Sn_{7.0}Sb_{5.0}$	$Sn_{1.2(2)}Pt_4Sn_{6.7(3)}Sb_{5.3(2)}$[a]	9.3915(4)
$Sn_{1.0}Pt_4Sn_{6.5}Sb_{5.5}$		9.3814(2)
$Sn_{1.0}Pt_4Sn_{6.0}Sb_{6.0}$	$Sn_{1.04(4)}Pt_4Sn_{5.92(4)}Sb_{6.08(6)}$	9.3779(2)
$Sn_{1.0}Pt_4Sn_{5.0}Sb_{7.0}$	$Sn_{1.0(2)}Pt_4Sn_{5.0(2)}Sb_{7.0(1)}$	9.3657(1)
$Sn_{1.0}Pt_4Sn_{4.0}Sb_{8.0}$	$Sn_{0.3(2)}Pt_4Sn_{4.3(2)}Sb_{7.7(1)}$	9.3371(3)
$Pt_4Sn_{7.0}Sb_{5.0}$	$Sn_{0.92(7)}Pt_4Sn_{6.64(7)}Sb_{5.36(6)}$	9.3905(4)
$Pt_4Sn_{6.0}Sb_{6.0}$	$Sn_{1.08(6)}Pt_4Sn_{5.64(6)}Sb_{6.36(6)}$	9.3719(4)
$Pt_4Sn_{5.0}Sb_{7.0}$	$Sn_{0.8(2)}Pt_4Sn_{4.6(2)}Sb_{7.4(2)}$[a]	9.3499(3)
$Sn_{0.91(5)}Pt_4Sn_{6.37(9)}Sb_{5.39(9)}$ (single crystal)	$Sn_{1.00(5)}Pt_4Sn_{6.63(5)}Sb_{5.37(4)}$	9.3887(1)

[a] EDXS data.

share in random distribution the 24*g* site, and the Sn atoms were found in the center of the cavity (site 2*a* (0 0 0)) having large displacement parameters.

In accordance with an early suggestion of Pauling for $CoAs_3$,[17] chemical bonding within the iron−antimony network in $NaFe_4Sb_{12}$ was shown to be directed (covalent) and different than the framework−filler interaction by applying the electron localizability tools. Sodium is playing the role of a cation, so that the total balance of electron counts may be written as $Na^{0.98+}[Fe_4Sb_{12}]^{0.98-}$.[18] The ionic interaction between the filler and host framework is often assumed for filled skutterudites within a Zintl-like model (see, e.g., ref 19).

Taking into account the interesting physical properties for tin-containing skutterudites,[20,21] we performed a systematic investigation of the Pt−Sn−Sb system, where a ternary phase $PtSn_{1.2}Sb_{1.8}$ with a crystal structure of the $CoAs_3$ type (a = 9.394 Å) was reported.[22] Obviously, the antimony-by-tin substitution at the framework site stabilizes the structural motif. In the present paper, we report on a ternary phase $Sn_xPt_4Sn_ySb_{12-y}$ ($0.3 \le x \le 1.0$ and $4.2 \le y \le 7.0$). The nature and the details of the filler's behavior will be discussed by means of the results of the crystal structure refinement and the nuclear magnetic resonance (NMR) measurements. Chemical bonding is analyzed by using the electron localizability indicator. The magnetism and electrical resistivity of $Sn_xPt_4Sn_ySb_{12-y}$ are characterized.

Experimental Section

Starting materials for the preparation of samples $Sn_xPt_4Sn_ySb_{12-y}$ were platinum foil (99.9 mass %, ChemPur), tin granules (99.99 mass %, ChemPur), and antimony granules (99.999 mass %, ChemPur). Bulk alloys were synthesized by arc melting of the elements in appropriate amounts on a water-cooled copper hearth in an argon atmosphere. Total mass losses of less than 1% were attributed to the evaporation of antimony and were precompensated. Because of the large difference in the melting temperatures between platinum and tin/antimony, the arc-melted samples contained several phases including the nonreacted platinum particles. Thus, the premelted samples were ground and cold-pressed to pellets, put into carbon crucibles, sealed in silica tubes filled with argon (600 mbar), and annealed at 700 °C for 24 h, then they were cooled to 500 °C for 24 h and annealed at this temperature for one week. For achieving final homogeneity, the resulting products were reground again and powdered using ball milling, filled into a carbon die, and spark-plasma sintered (SPS) at 400 °C for 2 h in an argon atmosphere.[23] In the SPS setup, the temperature is measured in the wall of the graphite die. The real temperature of the sample during SPS treatment is higher, being in the region of 500 °C. This temperature was chosen for the homogenization treatment in respect

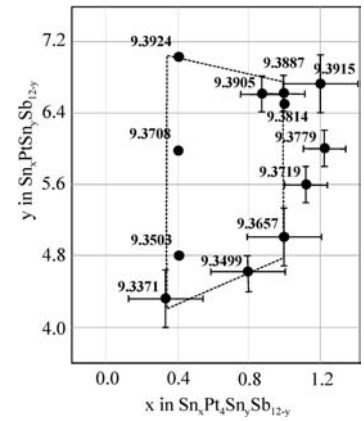

Figure 1. Lattice parameter of $Sn_xPt_4Sn_ySb_{12-y}$ as a function of the composition. The dotted line shows the homogeneity range of the phase. For the data points without error bars (where no chemical analysis was performed), the starting composition is used.

Table 2. Crystallographic Data and Details of the Crystal Structure Determination of $Sn_{0.91}Pt_4Sn_{6.37}Sb_{5.39}$

space group	$Im\bar{3}$ (no. 204)
formula units per unit cell	$Z = 2$
composition	$Sn_{0.91(5)}Pt_4Sn_{6.37(9)}Sb_{5.39(9)}$
unit cell parameter *a* (powder diffraction)	9.3887(1) Å
unit cell volume	827.59(2) Å^3
calculated density	9.22 g/cm^3
data collection	Rigaku Spider; Ag Kα; (λ = 0.5608 Å, graphite monochromator)
measured range; $(\sin\theta/\lambda)_{max}$	$4.8° \le 2\theta \le 122.6°$; 1.56
no. of measured reflections	9685
no. of symmetry independent reflections	2385
no. of reflections with $I > 2\sigma I$ used for refinement	1586
no. of refined parameters	28
absorption correction	numerical
absorption coefficient	29.18 mm^{-1}
extinction coefficient	0.0036(1)
$R_{gt}(F)$; $wR_{ref}(F^2)$	0.042/0.039

(14) Sellinschegg, H.; Stuckmeyer, S. L.; Hornbostel, M. D.; Johnson, D. C. *Chem. Mater.* **1998**, *10*, 1096–1101.
(15) Takizawa, H.; Miura, K.; Ito, M.; Suzuki, T.; Endo, T. *J. Alloys Compd.* **1999**, *282*, 79–83.
(16) Grytsiv, A.; Rogl, P.; Berger, St.; Paul, Ch.; Michor, H.; Bauer, E.; Hilscher, G.; Godart, C.; Knoll, P.; Musso, M.; Lottermoser, W.; Saccone, A.; Ferro, R.; Roisnel, T.; Noël, H. *J. Phys.: Condens. Matter* **2002**, *14*, 7071–7090.
(17) Pauling, L. *Can. Mineral.* **1978**, *16*, 447–452.
(18) Leithe-Jasper, A.; Schnelle, W.; Rosner, H.; Baenitz, M.; Rabis, A.; Gippius, A. A.; Morozova, E. N.; Borrmann, H.; Burkhardt, U.; Ramlau, R.; Schwarz, U.; Mydosh, J. A.; Grin, Yu. *Phys. Rev. B: Condens. Matter Mater. Phys.* **2004**, *B70*, 214418(1−11).
(19) Sales, B. C. Filled Skutterudites. In: *Handbook of the Physics and Chemistry of the Rare Earths*; Elsevier: New York, 2002; Vol. *33*, pp 1−34.
(20) Nolas, G. S.; Cohn, J. L.; Slack, G. A. *Phys. Rev. B: Condens. Matter Mater. Phys.* **1998**, *58*, 164–170.
(21) Dilley, N. R.; Bauer, E. D.; Maple, M. B.; Sales, B. C. *J. Appl. Phys.* **2000**, *88*, 1948–1951.
(22) Bhan, S.; Gödecke, T.; Schubert, K. *J. Alloys Compd.* **1969**, *19*, 121–140.

Table 3. Atomic Coordinates and Displacement Parameters in the Crystal Structure of $Sn_{0.91(5)}Pt_4Sn_{6.37(9)}Sb_{5.39(9)}$

atom	site	x	y	z	occ.	U_{11}	U_{22}	U_{33}	U_{12}	U_{13}	U_{23}	U_{eq}
Pt	8*c*	1/4	1/4	1/4		0.00686(3)	U_{11}	U_{11}	0.00152(3)	U_{12}	U_{12}	0.00686(2)
Sb	24*g*	0.35450(8)	0	0.15801(1)	0.449(7)	0.0125(2)	0.0068(2)	0.0103(2)	0	0.0021(2)	0	0.00987(1)
Sn1	24*g*	0.33395(7)	0	0.15284(8)	0.531(8)	0.0131(2)	0.0057(2)	0.0083(2)	0	0.00063(1)	0	0.00905(1)
Sn2	48*h*	0.076(1)	0.021(1)	0.076(1)	0.038(2)	0.029(5)	0.038(7)	0.030(5)	−0.012(5)	−0.010(3)	−0.007(4)	0.032(3)

of the relatively low decomposition temperature of the skutterudite phase (626 °C, see below). Single crystals were prepared by heating of the tin-rich flux at 700 °C for 12 h, then the melt was cooled at a rate of 5 °C/h to 400 °C and kept at this temperature for 24 h. Excess tin was removed by hot centrifugation[24] at 400 °C and subsequent treatment with a hot solution of HCl (37%) to dissolve impurities on the surface of the crystals.

Thermal behavior was studied using a differential thermal analysis (DTA) STA 409C (Netzsch) apparatus. For DTA measurements, the samples were sealed in niobium ampoules and heated at a rate of 10 °C/min in the temperature range between room temperature and 900 °C under flowing argon.

The phase appearance in the microstructure of the samples was studied by optical metallography. The chemical composition of the phases was analyzed by means of scanning electron microscopy (Philips XL30) and electron microprobe (Cameca SX 100) by energy-dispersive and wavelength-dispersive X-ray analysis (EDXS and WDXS), respectively. Quantitative analyses were performed on a microprobe using the WDXS method with an electron beam of 15 keV/100 nA and 25 kV/10 nA for excitation. Large monochromator crystals, LPC3 ($2d$ = 198 Å), LPET ($2d$ = 8.75 Å), and LLIF ($2d$ = 4.027 Å), were used to focus the appropriate fluorescence X-ray line on the proportional counters. The following elements or compounds with well-defined chemical composition were used as references: Sn, Sb, and $LaPt_2$.

Samples characterization was done by X-ray powder diffraction using the Guinier technique (Huber Image Plate Camera G670, Cu $K\alpha_1$ radiation with λ = 1.54056 Å, 5° < 2θ < 100°, step width 0.005 ° of 2θ, LaB_6 as an internal standard, a = 4.15692 Å). Unit cell parameters were refined with the WinCSD software.[25] The Rigaku Spider diffraction system (Ag Kα radiation, λ = 0.5608 Å) was used for the intensity data collection of the single crystal. The crystal structures were solved by direct methods and refined using the SHELX-97[26] and WinCSD program packages.[25]

Magnetization (M) of the samples was measured in various magnetic fields (H_{ext}) up to 70 kOe and for temperatures in the range of 1.8−400 K in a SQUID magnetometer (MPMS-XL7, Quantum Design). Electrical resistivity was investigated on specimens cut out from compacted samples of $Sn_xPt_4Sn_ySb_{12-y}$ prepared by SPS and single crystals of $Sn_{0.91}Pt_4Sn_{6.37}Sb_{5.39}$ within the temperature range from 4 to 300 K applying four-probe techniques.

Broad-line NMR measurements were carried out at 4.3 K using a commercial pulse NMR spectrometer (Tecmag). The spectra are obtained by the field-sweep method using a fixed frequency of about 70 MHz.

Table 4. Interatomic Distances (in Å) in $Sn_{0.91}Pt_4Sn_{6.37}Sb_{5.39}$

Atoms			Distance
Pt	- 6	Sn1	2.6387(3)
		Sb	2.6866(4)
	- 2	Sn2	3.16(1)
			3.44(1)
Sn1	- 1	Sn2	2.53(1)
	- 2	Pt	2.6387(3)
	- 2	Sn1	2.870(1)
		Sb	2.925(1)
Sb	- 1	Sn2	2.73(1)
	- 2	Pt	2.6866(4)
	- 2	Sb	2.732(1)
		Sn1	2.925(1)
Sn2	- 1	Sn1	2.53(1)
		Sb	2.73(1)
	- 1	Sn1	2.81(1)
		Sb	3.00(1)
	- 1	Sn1	3.01(1)
		Sb	3.19(1)
	- 1	Sn1	3.11(1)
		Sb	3.24(1)

Electronic structure calculation and bonding analysis were carried out using the TB-LMTO-ASA program package.[27] The Barth−Hedin exchange potential[28] was employed for local-density approximation calculations. The radial scalar-relativistic Dirac equation was solved to get the partial waves. Although the calculation within the atomic

(23) (a) Grin, Yu.; Reinfried, N.; Sebastian C. P.; Höhn, P.; Budnyk, S.; Leithe-Jasper, A.; Recknagel, C.; Li-ang, Y.; Friedemann, G.; Tokita, M. *7th Pacific Rim Conference on Ceramics and Glass Technology, Book of Abstracts*; 2007; p 170. (b) Reinfried, N.; Höhn, P.; Grin, Yu. *Scientific Report MPI CPfS*; 2005; pp 28−31.

(24) (a) Fisk, Z.; Remeika, J. P. In *Handbook on the physics and chemistry of the rare earths*; Gschneider, K. A., Eyring, L. R., Eds.; North-Holland: Amsterdam, 1989; Vol. *12*, pp 53−70. (b) Boström, M.; Hovmöller, S. *J. Alloys Compd.* **2001**, *314*, 154–159.

(25) Akselrud, L. G.; Zavalij, P. Yu.; Grin, Yu.; Pecharsky, V. K.; Baumgartner, B.; Woelfel, E. *Mater. Sci. Forum* **1993**, *133−136*, 335–340.

(26) Sheldrick, G. M. *SHELXL-97*; University of Göttingen: Göttingen, Germany, 1997.

(27) Jepsen, O.; Burkhardt, A.; Andersen, O. K. *TB-LMTO-ASA*, version 4.7; Max-Planck Institut für Festkörperforschung: Stuttgart, Germany, 1999.

(28) Barth, U.; Hedin, L. *J. Phys. C* **1972**, *5*, 1629–1642.

(29) Andersen, O. K. *Phys. Rev. B: Condens. Matter Mater. Phys.* **1975**, *12*, 3060–3083.

(30) Space group $P1$, $a = b = c$ = 9.3779 Å, $\alpha = \beta = \gamma$ = 90°, all atoms in the general 1(*a*) site with the following atomic coordinates and sphere radii: Pt1 (0.2500, 0.2500, 0.2500), r = 1.745 Å; Pt2 (0.2500, 0.2500, 0.7500), r = 1.746 Å; Pt3 (0.2500, 0.7500, 0.7500), r = 1.745 Å; Pt4 (0.2500, 0.7500, 0.2500), r = 1.745 Å; Pt5 (0.7500, 0.7500, 0.2500), r = 1.745 Å; Pt6 (0.7500, 0.7500, 0.7500), r = 1.745 Å; Pt7 (0.7500, 0.2500, 0.7500), r = 1.739 Å; Pt8 (0.7500, 0.2500, 0.2500), r = 1.739 Å; Sn1−1 (0.5000, 0.6528, 0.8339), r = 1.817 Å; Sn1−2 (0.8340, 0.5000, 0.3472), r = 1.818 Å; Sn1−3 (0.6528, 0.8340, 0.5000), r = 1.711 Å; Sn1−4 (0.8340, 0.5000, 0.6528), r = 1.818 Å; Sn1−5 (0.1528, 0.3340, 0.0000), r = 1.818 Å; Sn1−6 (0.3340, 0.0000, 0.1528), r = 1.818 Å; Sn1−7 (0.6528, 0.1661, 0.5000), r = 1.824 Å; Sn1−8 (0.8432, 0.3340, 0.0000), r = 1.807 Å; Sn1−9 (0.1661, 0.5000, 0.6528), r = 1.817 Å; Sn1−10 (0.3340, 0.0000, 0.8472), r = 1.818 Å; Sn1−11 (0.0000, 0.8472, 0.3340), r = 1.818 Å; Sn1−12 (0.0000, 0.1528, 0.6661), r = 1.817 Å; Sn1−13 (0.5000, 0.6580, 0.1455), r = 1.882 Å; Sb1−1 (0.0000, 0.8420, 0.6455), r = 1.882 Å; Sb1−2 (0.6455, 0.0000, 0.8420), r = 1.883 Å; Sb1−3 (0.6455, 0.0000, 0.1580), r = 1.883 Å; Sb1−4 (0.8420, 0.6455, 0.0000), r = 1.883 Å; Sb1−5 (0.1455, 0.5000, 0.3420), r = 1.882 Å; Sb1−6 (0.3420, 0.1455, 0.5000), r = 1.844 Å; Sb1−7 (0.5000, 0.3420, 0.1455), r = 1.844 Å; Sb1−8 (0.0000, 0.1580, 0.3545), r = 1.882 Å; Sb1−9 (0.5000, 0.3420, 0.8545), r = 1.844 Å; Sb1−10 (0.1580, 0.6455, 0.0000), r = 1.882 Å; Sb1−11 (0.3420, 0.8545, 0.5000), r = 1.844 Å; Sn2 (0.5764, 0.5759, 0.5209), r = 1.711 Å. For the "ideal" model, the Sn2 atom was located at (0.5000, 0.5000, 0.5000) with r = 2.082 Å.

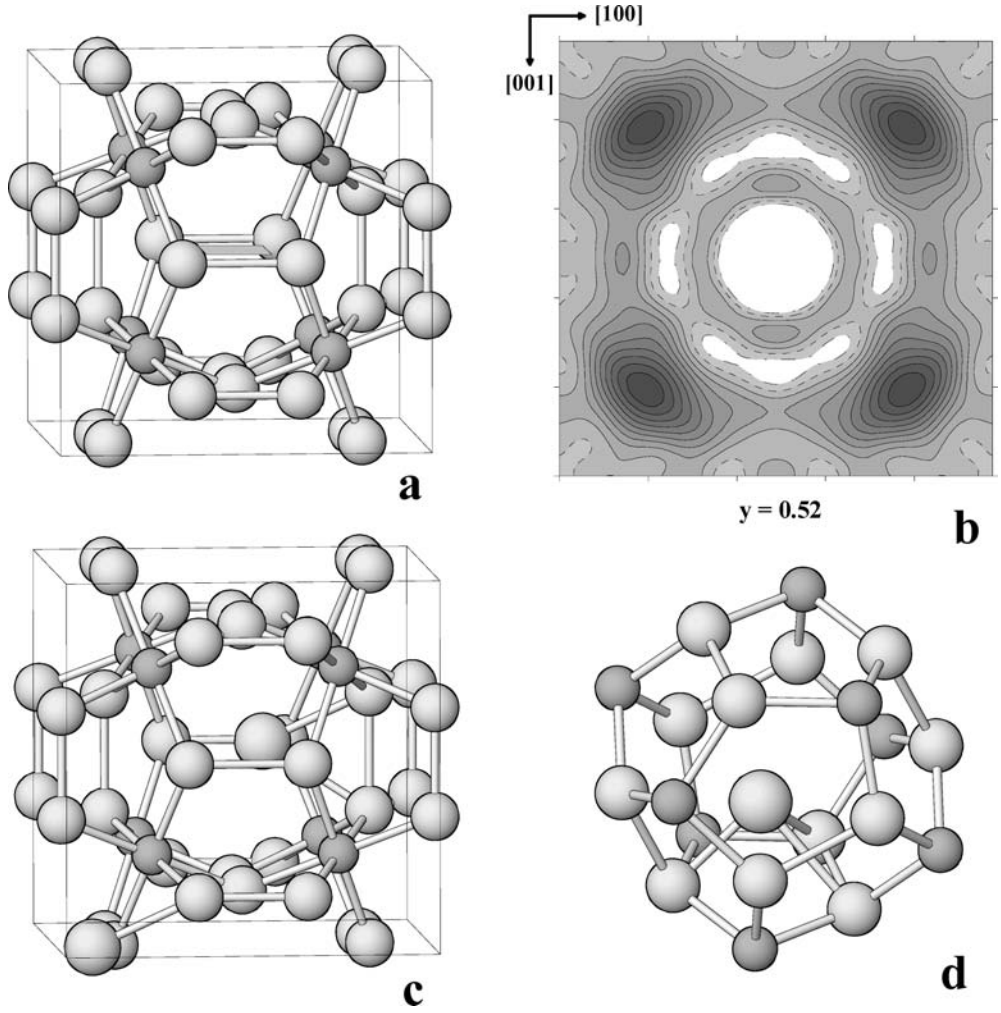

Figure 2. Crystal structure of $Sn_{0.91}Pt_4Sn_{6.37}Sb_{5.39}$: (a) The platinum atoms (dark gray spheres) are octahedrally coordinated by Sb/Sn1 atoms (light gray spheres) in the framework; the gray polygon represents the difference electron density map shown in Figure 2b. (b) The difference electron density in the plane around the point (0, 0.52, 0); the area shown has a size of 1 Å × 1 Å. (c) Sn2 atoms (light gray large spheres) occupy icosahedral voids with a shift from the center of the cavity. (e) Within the void, Sn2 atoms are bonded to three Sb/Sn1 atoms of the framework.

sphere approximation includes corrections for the neglect of interstitial regions and partial waves of higher order,[29] an addition of empty spheres was not necessary. The radii of the atomic spheres applied for the calculations are given in ref 30. A basis set containing Pt(6s,6p,5d), Sn(5s,5p), and Sb(5s,5p) orbitals was employed for a self-consistent calculation with Pt(5d), Sn(5d,4f), and Sn(5d,4f) functions being downfolded.

The electron localizability indicator (ELI; *Y*) was evaluated according to ref 31 with an ELI module implemented within the TB-MTO-SA package. The topology of ELI was analyzed using the program Basin,[32] with consecutive integration of the electron density in basins, which are bound by zero-flux surfaces in the electron localization function gradient field. This procedure, similar to the one proposed by Bader for the electron density,[33] allows assignment of an electron count for each basin, revealing additional information on chemical bonding.

Results and Discussion

For the determination of the homogeneity range of the new phase $Sn_xPt_4Sn_ySb_{12-y}$, a series of samples with $x = 0$, 0.4, and 1.0 and $4 \leq y \leq 7$ was used (Table 1). The preparation resulted in dark-gray bulk reguli with at least 90% of the theoretical mass density. The composition of the target phase after preparation was established by WDXS and EDXS analyses, whereby it was assumed that the framework position is completely occupied by tin and antimony atoms, and the excess tin atoms are located at the filler position (Table 1). Powder X-ray diffraction patterns reveal in all samples the majority phase with a body-centered cubic unit cell. The lattice parameter varies strongly with composition, indicating a large homogeneity range of the phase. The unit cell is expanding as the concentration of tin increases in the framework with a constant filler content, and in the filler position at a constant framework content (Figure 1 and Table 1). This is in agreement with the emptying of the bonding states (cf., density of states, DOS, below), which seems to have a stronger influence than the usual size factor (r_{Sn} = 1.58 Å, r_{Sb} = 1.61 Å[34]). DTA measurement of the annealed sample $Sn_{0.92}Pt_4Sn_{6.64}Sb_{5.36}$ (WDXS composition) reveals an endothermic peak upon heating at 263 °C caused by the melting of the tin-rich eutectic. Two further endothermic

(31) Kohout, M. *Int. J. Quantum Chem.* **2004**, *97*, 651–658.
(32) Kohout, M. *Basin*; version 4.2; 2007.
(33) Bader, R. F. W. *Atoms in molecules: a quantum theory*; Oxford University Press: Oxford, 1999.
(34) Emsley, J. *The Elements*; Clarendon Press: Oxford, 1989.

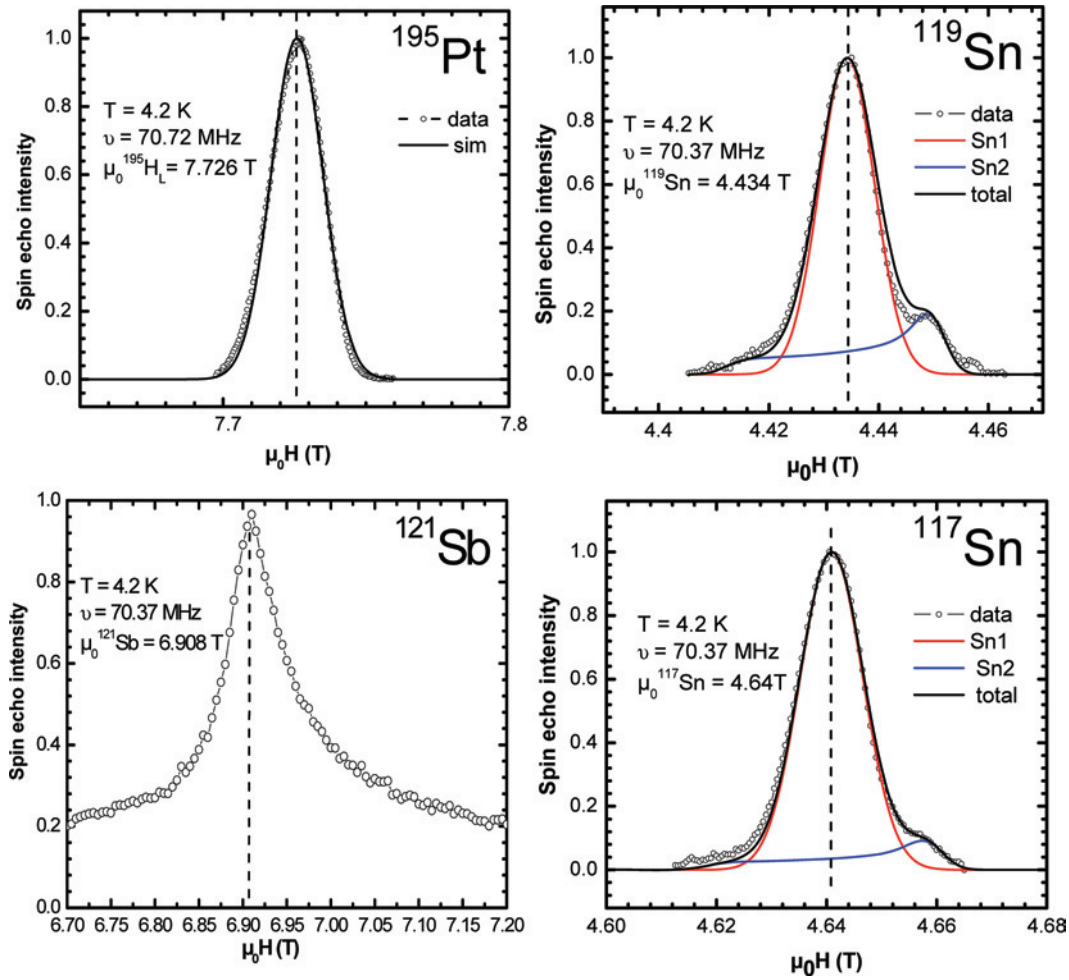

Figure 3. Nuclear magnetic resonance spectra for $Sn_{0.91}Pt_4Sn_{6.37}Sb_{5.39}$. Larmor fields of the nuclei are indicated by dashed vertical lines.

peaks at 626 and 980 °C correspond to the peritectic formation of the skutterudite phase and to the liquidus. After annealing for 21 days above the first temperature, the skutterudite phase decomposes into $PtSb_2$ and some unidentified phases. Thus, the phase $Sn_xPt_4Sn_ySb_{12-y}$ forms peritectically at 626 °C and has a concentration range of $0.3(2) \leq x \leq 1.0(2)$ and $4.2(2) \leq y \leq 7.0(2)$.

The silvery metallic crystals prepared from the tin flux (starting composition $SnPt_4Sn_7Sb_5$+4Sn) are stable in the air and do not react with concentrated HCl acid. The chemical composition of the crystals as concluded from the structure refinement corresponds to $Sn_{0.91(5)}Pt_4Sn_{6.37(9)}Sb_{5.39(9)}$, which agrees well with the composition $Sn_{1.00(5)}Pt_4Sn_{6.70(5)}Sb_{5.37(4)}$ obtained from WDXS. Details of data collection, structure determination, and refinement are presented in Table 2.

The final values of the atomic coordinates and the displacement parameters in the crystal structure of $Sn_{0.91(5)}Pt_4Sn_{6.37(9)}Sb_{5.39(9)}$ are summarized in Table 3; Table 4 presents the interatomic distances. The Sn and Sb atoms are randomly located at the 24*g* (*x* 0 *z*) position. The atomic coordinates *x* and *z* of Sn and Sb are slightly different because of the different size of antimony and tin atoms. Independent refinement of the site occupation parameters (the quality of the data set allows this, cf. Table 2) for both subpositions yielded the ratio 0.449(7):0.531(8), which shows full occupation of the framework position within 2 estimated standard deviations. Thus, thereafter, it will be considered as completely occupied. The Sn/Sb framework offers several types of voids (icosahedral, cuboctahedral, octahedral, and trigonal prismatic[35]) which may be filled by guest atoms. The octahedral voids are filled by Pt atoms located on the 8*c* (1/4 1/4 1/4) position, forming tilted corner-sharing octahedrons $Pt(Sn/Sb)_6$, in which the distances Pt−Sb and Pt−Sn are 2.6866 Å and 2.6387 Å, respectively (cf. Figure 2a and Table 3). The Pt−Sb distance is quite close to d(Pt−Sb) = 2.67 Å in $PtSb_2$ (structure type FeS_2).[36] The Pt−Sn distance is smaller than the observed values in the binary compounds: d(Pt−Sn) = 2.78 Å in $PtSn_2$ (structure type CaF_2), d(Pt−Sn) = 2.77 Å in $PtSn_4$ (own structure type).[36] This may be understood accounting for the larger CN = 8 for Pt with a cubic ($PtSn_2$) or tetragonal antiprismatic ($PtSn_4$) environment in the binary compounds.

Generally, filled skutterudites are characterized by an anomalously large isotropic atomic displacement for the filler atoms at the 2*a* (0 0 0) position (center of the icosahedral

(35) Gladyshevsky, R. E.; Grin, Yu.; Yarmolyuk, Ya. P.; *Dopov. Akad. Nauk Ukr. RSR, Ser. A*; **1997**, no. 2. 67–70.
(36) Breese, N. E.; von Schnering, H. G. *Z. Anorg. Allg. Chem.* **1994**, *620*, 393–404.
(37) Durussel, P.; Massara, R.; Feschotte, P. *J. Alloys Compd.* **1994**, *215*, 175–179.
(38) Schnelle, W.; Leithe-Jasper, A.; Rosner, H. R.; Cardoso, G.; Gumeniuk, R.; Trots, D.; Mydosh, J. A.; Grin, Yu. *Phys. Rev. B: Condens. Matter Mater. Phys.* **2008**, *77*, 094421(1−16).

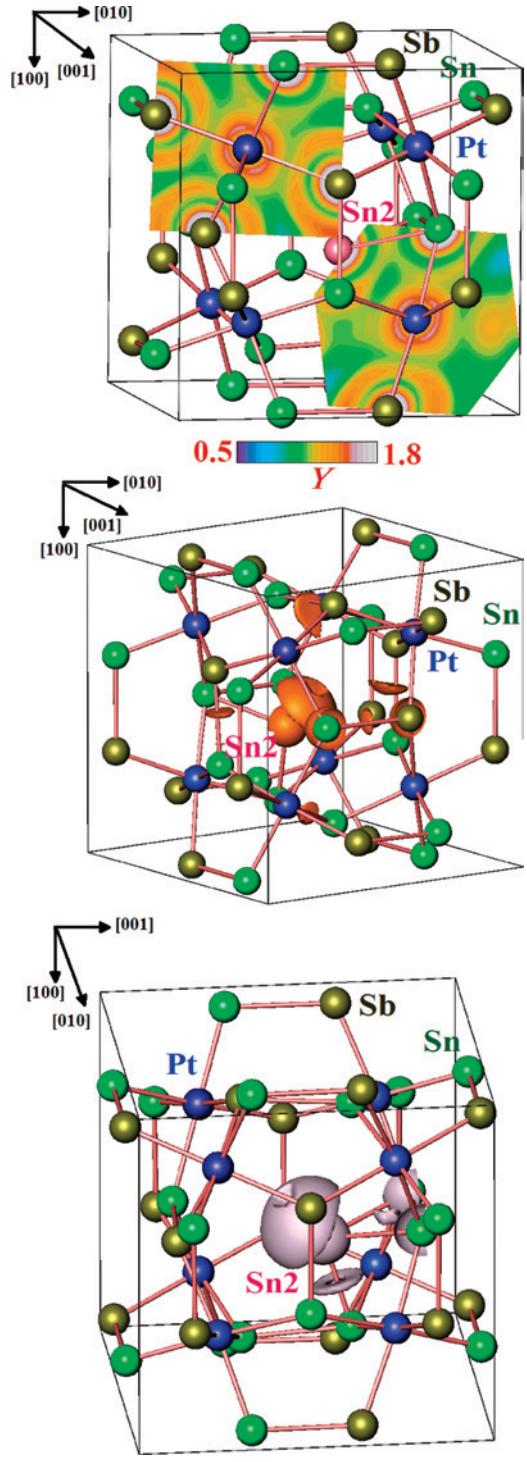

Figure 4. Electron localizability indicator (Y) in $Sn_{0.5}Pt_4Sn_{6.5}Sb_{5.5}$: (top) sections of ELI show the structuring of the penultimate shells for the Pt atoms in the vicinity of Sn2 (right) and far from Sn2 (left). (middle) The isosurface with $Y = 1.37$ visualizes Sn−Sb bonds within the framework and the "lone pair" on Sn1. (bottom) The isosurface with $Y = 1.255$ shows the interaction of Sn2 with the framework—"lone pair", 2c bond Sn2−Sn, 3c bond Sn2−Sn−Sb.

hole of the Sn/Sb framework), especially in the antimonides $Sn_{1-x}Co_4Sb_{12}$,[15] $Sn_{0.31}Ni_4Sn_{5.6}Sb_{6.4}$,[16] and AFe_4Sb_{12}.[38] In the case of $Sn_{0.91}Pt_4Sn_{6.37}Sb_{5.39}$, the electron density in the vicinity of the 2a position (Figure 2b) reveals clearly the location of the filler atom out of the center of the cavity in the general 48h (x y z) site (Figure 2c). Instead of having 12 ligands at

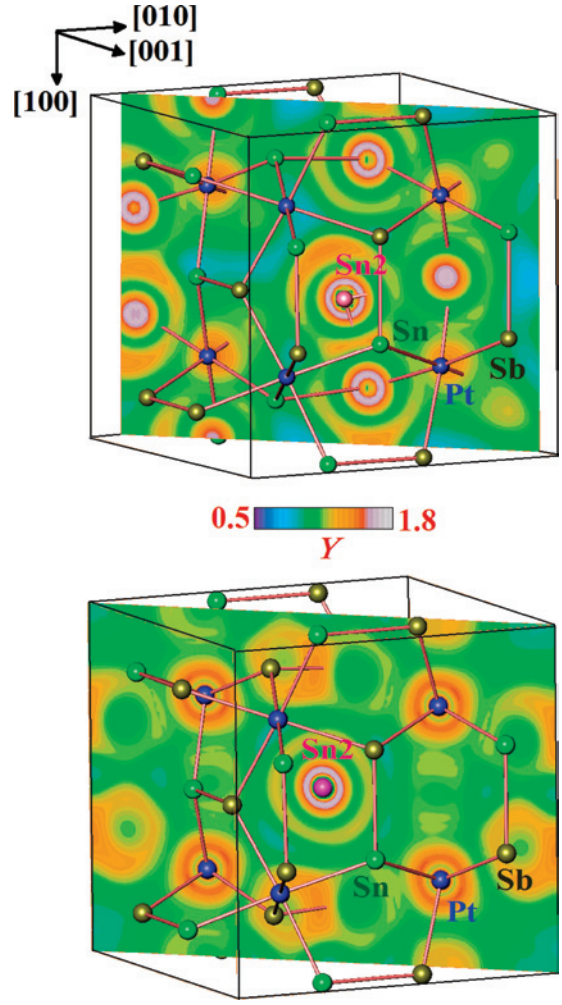

Figure 5. Electron localizability indicator (Y) in $Sn_{0.5}Pt_4Sn_{6.5}Sb_{5.5}$: The section of ELI shows the strong structuring of the valence shell for Sn2 on the experimentally found position (top) and the weak structuring for the ideal position 1/21/21/2 (bottom).

the same distance being in the center of the cavity, the filler atoms form three short distances to Sn1 (2.53, 2.81, 3.01 Å) or Sb atoms (2.73, 3.00, 3.19 Å), forming vertices of a distorted tetrahedron (Figure 2d). The next nearest distance is larger (3.11 Å for Sn1 or 3.24 Å for Sb).

In fact, the refinement of the site occupation factor for the filler position (Sn2) yielded only a scattering factor of roughly one electron at this point (48 electrons in total for the site). They may be realized by partial occupation of any of the constituents (platinum, antimony, or tin). The sort of filler atom and the local ordering was finally established by NMR measurements. The ^{195}Pt NMR ($I = 1/2$) signal (Figure 3, top) does not reveal special features, which is in agreement with an antimony and tin environment of the platinum atoms which is close to octahedral symmetry (cf. small difference in the interatomic distances between Pt and Sb or Sn1, above). The ^{121}Sb NMR ($I = 5/2$) signal reveals an enlarged width, which is in agreement with a possible disorder of Sn and Sb atoms being in contact with Sb atoms. In contrast, the ^{117}Sn and ^{119}Sn NMR ($I = 1/2$) signals clearly show a double-peak structure, suggesting two different environments of the tin atoms in the crystal structure with the lower symmetry for the second one, which is in full agreement

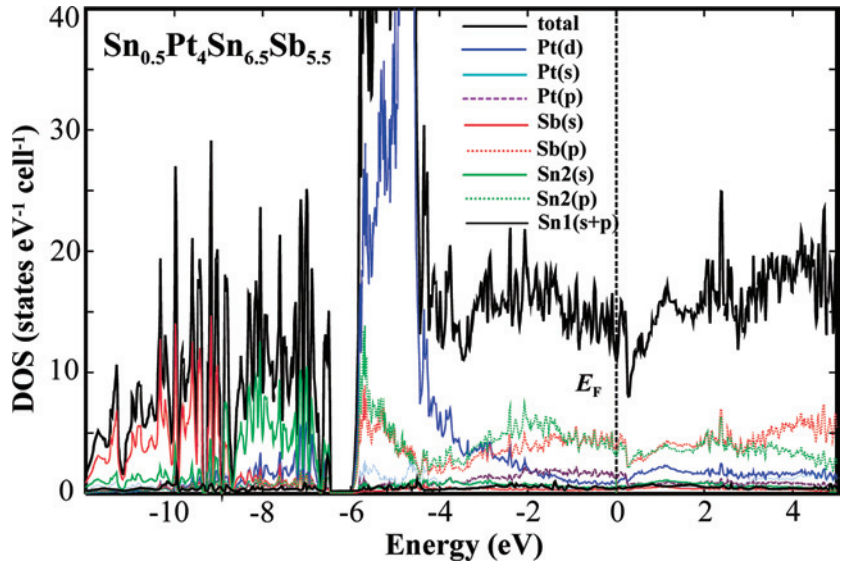

Figure 6. Calculated electronic density of states for $Sn_{0.5}Pt_4Sn_{6.5}Sb_{5.5}$ with partial contributions of Pt, Sb, Sn1, and Sn2 atoms.

with the crystallographic data. The average (for ^{117}Sn and ^{119}Sn signals) intensity ratio of the signals (5.2:1) is somewhat reduced in comparison with the crystallographic data (12:1). Nevertheless, this finding allows assignment of the low-field signal to the framework (Sn1) position, whereby the lower-intensity high-field signal reflects the filler (Sn2) position.

A strong shift of the Sn2 atoms away from the center of the cavity, where filler atoms are usually found in filled skutterudites, suggests a different chemical interaction in $Sn_xPt_4Sn_ySb_{12-y}$ compared to other compounds of this class. This was one of the reasons for performing an analysis of the chemical bonding using ELI.[31] For the ELI calculation, an ordered model with composition $Sn_{0.5}Pt_4Sn_{6.5}Sb_{5.5}$ was derived in space group $P1$.[30] The Sn/Sb ratio was chosen as close as possible to the value evaluated from crystal structure determination within a unit cell of the same size. Only one of the two cavities in the unit cell was filled for modeling the defect occupancy of the filler position. Within the framework, homonuclear Sb−Sb or Sn−Sn contacts were omitted in the model as much as possible. In order to evaluate the influence of the filler displacement, two models were calculated: one with and one without shift (the Sn2 atom was located either in the center of the cavity or in the experimentally determined position). The second one is called hereafter "ideal". The atomic coordinates were taken from the crystal structure determination without optimization.

For both models, the distribution of ELI in the vicinity of the platinum atoms reveals a strong structuring of the penultimate shell. Compared with a spherical distribution, ELI shows reduced values in the direction of the neighboring tin/antimony atoms and increased values toward the middle of the $(Sb,Sn1)_3$ triangular face of the $Pt(Sn,Sb)_6$ octahedron. This picture is independent of the fact of whether the Sn2 atom is in the vicinity of the Pt or not (Figure 4, top). The structuring of the penultimate shell is a fingerprint of a direct atomic interaction.[39,40] Interestingly, there are no maxima found on the Pt−(Sn1,Sb) contacts, which were observed on such contacts in other filled skutterudites, for example, $NaFe_4Sb_{12}$.[18] Thus, the Pt−(Sn1,Sb) interactions are manifested solely by the structuring of the penultimate shell.[39,40]

Separate maxima of ELI were found on the Sn1−Sb contacts (Figure 4, middle) completing the covalent interactions within the Pt/(Sn1,Sb) framework. In the vicinity of the Sn2 atoms, ELI shows three types of attractors. The first one is located closely to the Sn2 core and may be considered as "lone-pair"-like (Figure 4, middle, bottom). The second one, a ring-like attractor, is located between Sn2 and Sn1, visualizing a two-center bond; the third one is positioned within the triangle formed by Sn2, Sn1, and Sb, revealing a three-center interaction (Figure 4, bottom). In total, ELI in the valence region of Sn2 being displaced is strongly structured (Figure 5, top) compared with the situation when Sn2 is located in the center of the cavity (Figure 5, bottom).

The calculated electronic density of states (Figure 6) for the ordered model with shift[30] shows quite strong structuring in the low-energy region ($E < -6$ eV). This region is mainly formed by s states of Sn and Sb, with small contributions of p states of Sn and Sb as well as s and p states of Pt, and reflects the bonding within the framework. Interestingly, the Sn(s) and Sb(s) contributions are separated; hereby, the Sn(s) states are located at higher energy. The region between −6 eV and −4 eV is formed almost exclusively by d states of Pt which are strongly localized. Only a small part of the d states contributes to the low-energy region ($E < -6$ eV), in agreement with the picture given by the ELI analysis. The region below the Fermi level (-4 eV $< E < E_F$) is formed mainly by the p states of Sb and Sn as well as by the d and p states of Pt. The Sb(p) and Sn(p) contributions at the Fermi level are practically equal. A pseudo-gap is observed slightly

(39) Kohout, M.; Wagner, F. R.; Grin, Yu. *Theor. Chem. Acc.* **2002**, *108*, 150–156.
(40) Wagner, F. R.; Bezugly, V.; Kohout, M.; Grin, Yu. *Chem.—Eur. J.* **2007**, *13*, 5724–5741.

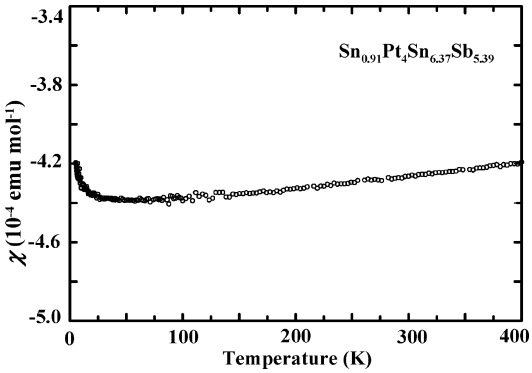

Figure 7. Magnetic susceptibility of $Sn_{0.91}Pt_4Sn_{6.37}Sb_{5.39}$ versus the temperature in a magnetic field of 35 kOe.

above the Fermi level ($E = 0.3$ eV). It suggests the possibility for further filling of the cavity or further replacement of the tin by antimony, which is in good agreement with the investigation of the homogeneity range (Sb-richest composition $Sn_{1.0}Pt_4Sn_{4.2}Sb_{7.8}$). From $E = -2$ eV to the pseudo gap, the DOS continuously decreases. The DOS at E_F is non-negligible (about 12 states/(eV unit cell)), indicating metallic electron transport behavior.

Because all components are nonmagnetic, the calculated DOS suggests also a diamagnetism of $Sn_xPt_4Sn_ySb_{12-y}$: 12 states/(eV unit cell) gives, according to ref 41, a paramagnetic susceptibility of 190×10^{-6} emu/mol. Taking into account the diamagnetic core contributions of -304×10^{-6} emu/mol for the composition $Sn_{0.91}Pt_4Sn_{6.37}Sb_{5.39}$, one obtains a total susceptibility of -104×10^{-6} emu/mol. This is in qualitative agreement with the measurement of the magnetic susceptibility of $Sn_{0.91}Pt_4Sn_{6.37}Sb_{5.39}$ (Figure 7), which exhibits diamagnetic behavior in the temperature range 1.8−400 K and an extrapolated value of -444×10^{-6} emu/mol for zero temperature. The minor paramagnetic impurities (0.0.03 μB f.u.$^{-1}$) probably originating from the starting materials cause the low-temperature up-turn in the magnetic susceptibility at $T < 30$ K.

The electrical resistivity of $Sn_xPt_4Sn_ySb_{12-y}$ is characterized by relatively large values of $\rho(T)$, which increase with the temperature (Figure 8). In agreement with the calculated electronic DOS, all of the samples show metallic behavior which is different than that of the skutterudite $Sn_xNi_4Sn_ySb_{12-y}$.[16] Here, the samples richest in Sn do not exhibit metallic behavior. For the skutterudite $Sn_xPt_4Sn_ySb_{12-y}$, the absolute resistivity tends to increase with increasing tin content.

Within the temperature range investigated, no special features were found in magnetic susceptibility and electrical resistivity which may be attributed to a lock-in process of the filler atom, if its off-center position would have a dynamic character. This gives additional support for the finding of a static nature of the filler position.

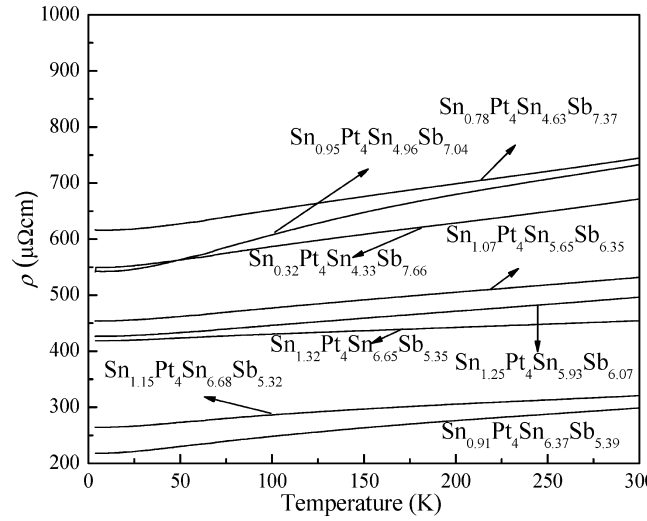

Figure 8. Temperature dependence of the electrical resistivity of $Sn_xPt_4Sn_ySb_{12-y}$ with different compositions.

Conclusions

A Pt-based skutterudite $Sn_xPt_4Sn_ySb_{12-y}$ has been synthesized and characterized. The lattice parameter refinements and the WDXS analyses revealed a wide range of homogeneity for $0.3(2) \leq x \leq 1.0(2)$ and $4.2(2) \leq y \leq 7.0(2)$. It is evident from single-crystal X-ray diffraction and NMR data that the Sn atoms occupy two crystallographically inequivalent sites: Sn and Sb atoms in random distribution share the framework site; a small fraction of Sn atoms occupy the icosahedral voids. In contrast to the known skutterudites, the filler Sn atoms are shifted from the center of the cavity. Analysis of the chemical bonding by the electron localizability indicator reveals direct (covalent) interactions between the filler and framework, this being observed for the first time in skutterudite-like compounds. In agreement with the calculated electronic DOS, $Sn_xPt_4Sn_ySb_{12-y}$ exhibits metallic conductivity and diamagnetic behavior.

Acknowledgment. The authors would like to express their gratitude to Drs. A. Leithe-Jasper and U. Schwarz for valuable discussions and thank Dr. S. Hoffmann for DTA, Mr. T. Vogel and Ms. M. Eckert for metallography and WDXS, Mr. R. Koban for susceptibility and resistivity measurements, and Mr. S. Hückmann for collecting powder diffraction data. Y.L. and J.T.Z. are in debt to the CAS-MPG Partner group program and to the National Research Program of China (grant no. 2007CB607503).

IC801154A

(41) Ashcroft, N. W.; Mermin, N. D. *Solid State Physics*; Hartcourt College Publishers: Forth Worth, TX, 1976; p 661ff.